Endoplasmic Reticulum Stress Induced by Zinc Oxide Nanoparticles Is an Earlier Biomarker for Nanotoxicological Evaluation

Rui Chen,[†,§] Lingling Huo,[†,‡,§] Xiaofei Shi,[†] Ru Bai,[†] Zhenjiang Zhang,[†] Yuliang Zhao,[†] Yanzhong Chang,[‡,*] and Chunying Chen[†,*]

[†]CAS Key Lab for Biomedical Effects of Nanomaterials and Nanosafety, National Center for Nanoscience & Technology of China, Beijing 100090, P. R. China and [‡]Laboratory of Molecular Iron Metabolism, College of Life Science, Hebei Normal University, Shijiazhuang 050016, P. R. China. [§]These authors contributed equally to this work.

ABSTRACT Zinc oxide nanoparticles (ZnO NPs) have been widely used in cosmetics and sunscreens, advanced textiles, self-charging and electronic devices; the potential for human exposure and the health impact at each stage of their manufacture and use are attracting great concerns. In addition to pulmonary damage, nanoparticle exposure is also strongly correlated with the increase in incidences of cardiovascular diseases; however, their toxic potential remains largely unclear. Herein, we investigated the cellular responses and endoplasmatic reticulum (ER) stress induced by ZnO NPs in human umbilical vein endothelial cells (HUVECs) in comparison with the Zn^{2+} ions and CeO_2 NPs. We found that the dissolved zinc ion was the most significant factor for cytotoxicity in HUVECs. More importantly, ZnO NPs at noncytotoxic concentration, but not CeO_2 NPs, can induce significant cellular ER stress response with higher expression of spliced *xbp-1*, *chop*, and *caspase-12* at the mRNA level, and associated ER marker proteins including BiP, Chop, GADD34, p-PERK, p-eIF2α, and cleaved Caspase-12 at the protein levels. Moreover, ER stress was widely activated after treatment with ZnO NPs, while six of 84 marker genes significantly increased. ER stress response is a sensitive marker for checking the interruption of ER homeostasis by ZnO NPs. Furthermore, higher dosage of ZnO NPs (240 μM) quickly rendered ER stress response before inducing apoptosis. These results demonstrate that ZnO NPs activate ER stress-responsive pathway and the ER stress response might be used as an earlier and sensitive end point for nanotoxicological study.

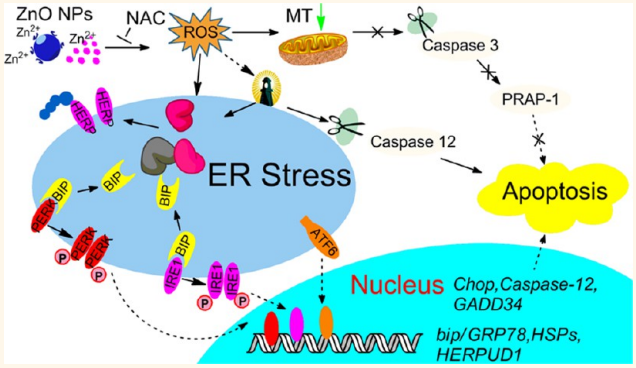

KEYWORDS: ZnO · ceria · nanoparticles · ER stress · signaling pathways · cytotoxicity · apoptosis

Safety concern on the engineered nanomaterials (ENMs) is rapidly expanding with the industrial level production and wide applications in consumer products.[1−3] Toxicity on the nanoparticles (NPs) of variant ENMs has been evaluated in different biological systems including animals, mammalian cells, model organisms, bacteria, and plants.[4−10] Generally, toxicological end points of the biological system, *i.e.*, inflammation, DNA damage, apoptosis, necrosis, fibrosis, hypertrophy, metaplasia, and carcinogenesis, are used in the toxic evaluation of ENMs.[11−15] These end points reflect the irreversible destiny of the tested biological system when being treated by ENMs at a toxic dosage level which can cause detectable effects. However, adverse effects still could be formed in the organism by showing as the interruption on the homeostasis before or even without forming obvious toxic phenotypes. The endoplasmic reticulum (ER) is an important organelle and functions in folding and assembling of cellular proteins, synthesis of lipids and sterols, and storage of free calcium, which are all dependent on the ER internal homeostasis.[16] ER stress also known as unfolded protein response (UPR), a well-studied issue in cell biology, refers to an important cellular self-protection mechanism which can be activated to counteract the stressed situation

* Address correspondence to chang7676@163.com, chenchy@nanoctr.cn.

Received for review December 2, 2013 and accepted February 3, 2014.

Published online February 03, 2014
10.1021/nn406184r

when in the condition of overloading unfolded proteins or even from direct ER damage.[17,18] ER stress usually happens for a short-term with provoking a series of transcriptional activities for cell survival, but prolonged ER stress activates apoptotic cell death pathways.[19−21]

Three transmembrane proteins, including inositol-requiring protein 1 (IRE1), PKR-like endoplasmic reticulum kinase (PERK), and activating transcription factor-6 (ATF-6), are stress-sensing proteins in the ER and in charge of giving signals to cellular self-recovery or, alternatively, promote cell death. The three stress-sensing proteins are held in inactive states by ER-chaperone protein 78 kDa glucose-regulated protein (GRP78/BiP) when organism is in normal state. When ER stress happens, BiP releases and leads stress-sensing proteins in an activating state. IRE1, one of the activated proteins, mediates removal of a 26 nucleotides long intron from X-box binding protein 1 (*xbp-1*) mRNA and introduces a frame-shift and an alternative C-terminus in the spliced form of *xbp-1* (*xbp-1s*). Then, *xbp-1s* translates into a potent transcription factor and translocates to the nucleus for initiating the transcription of *bip* and other cytoprotective genes. The induction of *bip* transcription and the *xbp-1* splicing are used as specific markers of ER stress response. It had been reported that the level of *xbp-1s* mRNA is a reliable and direct quantitative marker for the detection of ER stress.[22] CHOP (also known as DNA-damage-inducible transcript 3, DDIT3) and Caspase-12, not Caspase-3, are involved in ER stress related apoptosis which is caused from the unsuccessful self-recovery when activating ER stress pathway. Caspase-3 had been recognized as an active member in the mitochondria-initiated apoptosis pathway.[23]

It had been indicated that copper and copper oxide NPs could induce apoptosis through activating mitochondria mediated pathway.[24,25] However, Ag NP induces apoptosis *via* the modulation of ER stress reaction.[26,27] Recent report also showed that Ag NPs could lead to induction of ER stress in zebrafish with sequentially activating several consequences including the activation of apoptotic and inflammatory pathways.[28] ENMs including copper, copper oxide, and Ag NPs could induce cytotoxicity and trigger detectable toxicological end points *via* the generation of reactive oxygen species (ROS).[26−29] However, the relations between ROS producing ability and ER stress effects had not been clearly defined in toxic assessment on ENMs. Gold NP had been reported as an efficient cellular ER stress elicitor, although it is considered biocompatible with having various medical usages.[30] Furthermore, parallel experiment on $AgNO_3$ showed that the silver ion content may play important role in the induction of ER stress because silver is easily released from the surface of NPs in the culture medium.[31] ZnO is another important ENMs, which has about the third highest global production volume only after SiO_2 and TiO_2 among metal-containing ENMs.[32] It had been shown that toxicity was found for zinc oxide, but not ceria in mammalian cells. This toxicity is the result of zinc oxide nanoparticle dissolution leading to the release of toxic Zn^{2+}, which is capable of generating ROS,[33−35] while ceria nanoparticles could exhibit antioxidant activity by reversibly binding oxygen and shifting between the Ce^{3+} (reduced) and Ce^{4+} (oxidized) forms at the particle surface.[36,37] In this study, we investigated the toxic effects on ER stress response and following apoptosis by comparing zinc oxide and ceria NPs. Our results indicate that ZnO NPs could activate the ER stress pathway and even induce the apoptosis if the cells cannot counteract the adverse effects. Further, ER stress has the possibility to be used as an earlier, sensitive and valuable marker for nanotoxicological study.

RESULTS AND DISCUSSION

The mean crystallite diameters characterized by X-ray diffraction (XRD) spectra were 42 and 33 nm for ZnO and CeO_2, respectively, consistent with our transmission electron microscopy (TEM) observation (Figure 1A−C and Table 1). However, they were prone to agglomeration in the water as illustrated in the results of TEM images and nanoparticle tracking analysis (NTA) tests, which showed average sizes of about 100 nm even with sonication treatment before the test (Figure 1D,E). The agglomeration propensity of these NPs comes from the none-coating state and similarities of lower negative surface charge (Table 1).

We examined the toxic effects of various concentrations of ZnO and CeO_2 NPs in comparison with the $ZnCl_2$ to illustrate the possible toxicity effect of solubilized Zn^{2+} on HUVECs cells (Figure 2). Cell viability assay indicated that $ZnCl_2$ and ZnO NPs have a similar dose-dependent cytotoxicity when incubated with HUVECs for 24 h, with a little lower toxic effect of ZnO NPs than its counterpart Zn^{2+} from the concentration of 100 to 300 μM. At 240 μM, Zn^{2+} and ZnO NPs decreased the cellular viability to about 40% of the control. It had been proven that ZnO NP has a high solubility under aqueous conditions to form hydrated Zn^{2+}; the acidic conditions and the presence of biological components such as amino acids and peptides could increase this phenomenon.[33,38] Our results correlated to previous knowledge that Zn^{2+} solubilized from ZnO NPs contributing to the toxic effects, especially when using the uncoated particles.[33−35] In contrast, CeO_2 NPs did not show toxic effects even with doubling of tested dosage to 480 μM. As illustrated in the TEM images, more CeO_2 NPs were contained in the cellular cytoplasm than ZnO when incubating the HUVECs cells at the same safe dosage of 120 μM for 8 h (Figure 3A−C). This data agreed with the findings of ICP-MS: the uptake quantity of CeO_2 NPs was about 100 times higher than that of $ZnCl_2$ or ZnO NP (Figure 3D).

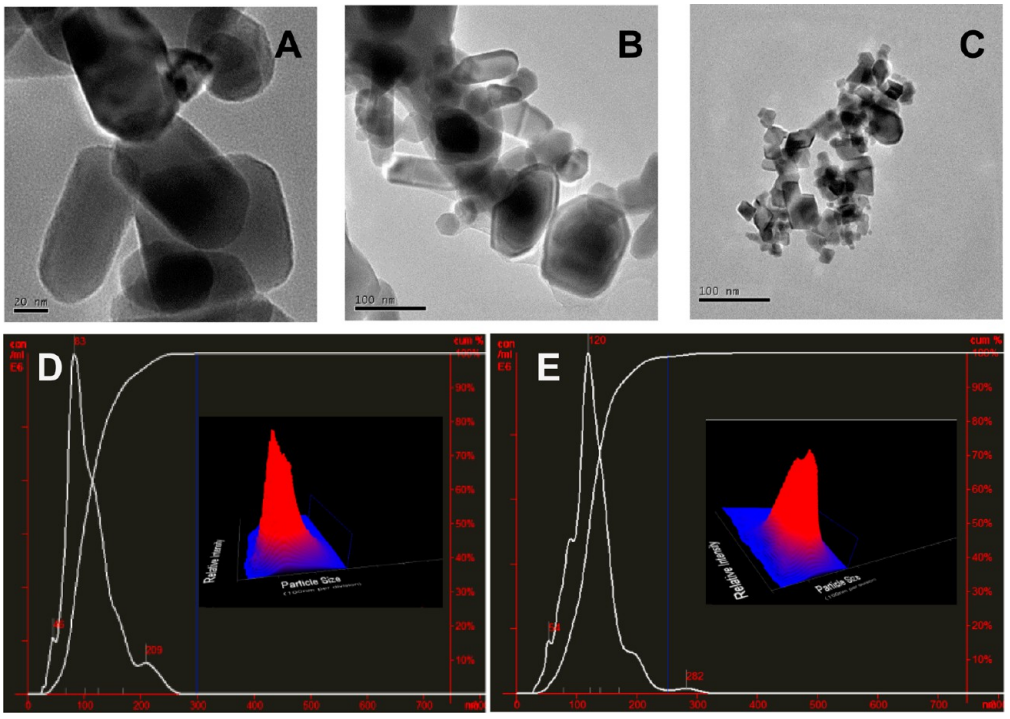

Figure 1. Characterization of ZnO and CeO_2 nanoparticles: (A and B) TEM images of ZnO NPs; (C) TEM image of CeO_2 NPs; (D) nanoparticle tracking analysis (NTA) result of ZnO NPs; (E) NTA result of CeO_2 NPs.

TABLE 1. Characterization of the Nanoparticles Used in This Study

nanoparticles	mean size (nm)[a]	primary crystal size by XRD (nm)[a]	$d_{h,water}$ (nm)[b]	zeta potentials (mV)[c]	coating[a]
ZnO (NM110)	150	42	111 ± 44	−6.14	None
CeO_2 (NM212)	28	33	125 ± 38	−6.64	None

[a] These parameters were provided by the supplier. [b] The $d_{h,water}$ value were measured by nanoparticle tracking analysis (NTA) method in Figure 1. [c] Surface charges were measured while the nanoparticles were dispersed in deionized water.

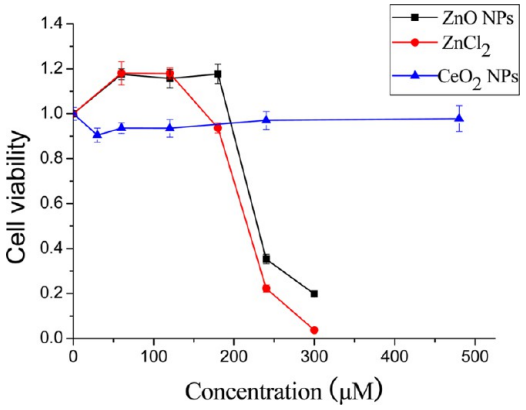

Figure 2. Cell viability assay of HUVECs when treated with different concentrations of ZnO NPs, CeO_2 NPs and $ZnCl_2$ for 24 h. The data represent the mean of at least three independent experiments normalized to untreated controls. Data expressed as mean ± SD, $n = 6$.

Furthermore, the number of mitochondria was significantly decreased, which correlated to the decreased activity of the cells, but had more obvious ERs showing a phenomenon of aggregation or swelling in ZnO NPs treated cells than for control and CeO_2 NPs treated groups (Figure 3B). ZnO NPs will decrease the cellular activity and take much more cellular internal damage especially to the ER compared to CeO_2 NPs, although it is not easy to scan the ZnO NPs by TEM.

Under normal circumstances, ROS is the byproduct of metabolism process and has an important role in cellular homeostasis.[39,40] However, this homeostasis can be easily disturbed by outer environmental stress. In this research, we checked intracellular ROS level by fluorescence microscopy. After incubation for 8 h, 240 μM ZnO NPs induced relatively higher levels of ROS in the cells compared to the blank control and the same dosage treated CeO_2 NP group (Figure 4A−L). At the same time, the ER within the ZnO NPs treated cells usually shows a little more obvious staining in an aggregated state. Quantitative analysis using high content analysis showed that ROS level of ZnO NPs treated group gave sharp increase when using dosages from higher than 120 μM, with 3.3-fold increase as the highest point comparing to the control (Figure 4N). However, CeO_2 NPs did not have a significant effect on the ROS level even at 480 μM concentration (Figure 4).

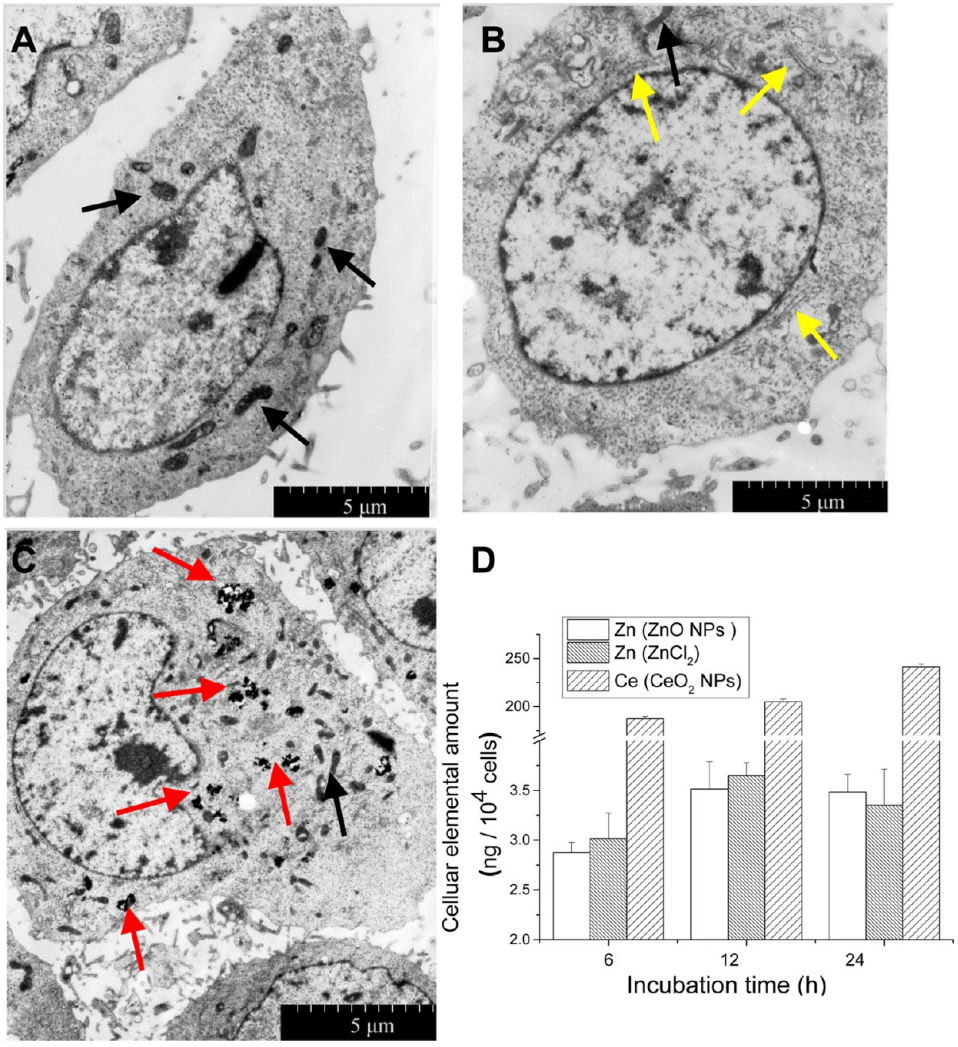

Figure 3. Endocytosis of NPs in HUVECs analyzed by TEM and ICP-MS. TEM images of HUVECs of (A) untreated control, (B) cells exposed to 120 μM ZnO or (C) cells exposed to 120 μM CeO_2 nanoparticles for 8 h. (D) Cellular uptake of HUVECs quantified by ICP-MS when incubated with 120 μM ZnO NPs, CeO_2 NPs, and $ZnCl_2$ for 6, 8, and 24 h, respectively. Black arrows show mitochondria, red arrows show the existence of CeO_2 NPs, and yellow arrows show the apparently aggregated or swelled endoplasmic reticulum in the cytoplasm of nanoparticle-treated cells.

The activation of ER stress pathway is a direct and quick outcome of the ER homeostasis interruption. So, this study focused on this signaling pathway after exposure to NPs. We checked the ER stress level by quantitative real-time PCR method on *xbp-1s* mRNA when incubating HUVECs cells with ZnO NPs at 120 μM concentration at which no obvious toxic effects in CCK assay were shown, but were starting to generate significant ROS in the cells (Figure 2 and Figure 4N). The *xbp-1s* mRNA levels were significantly increased by ZnO NPs and $ZnCl_2$ treatment, but not by CeO_2 NPs (Figure 5A,B). ROS generation should be involved in the induction of ER stress response within the ZnO NPs and $ZnCl_2$ treatment groups, as a widely used antioxidant *N*-acetylcysteine (NAC) pretreatment abolished the splicing of the *xbp-1* mRNA. The *xbp-1s* mRNA increased to the highest level at 8 h compared to the time points of 4 and 12 h, which means that the ER stress is at the highest level at that time point (Figure 5A). As another hallmark of ER stress responses, *chop* showed a similar increase profile by activation of ZnO NP and $ZnCl_2$ (Figure 5B). It had been reported that Caspase-12, as an executor of apoptosis, is localized to the ER and activated by ER stress, but not by membrane- or mitochondrial-targeted apoptotic signals.[21] After increasing the ZnO NPs to 240 μM concentration, cleaved Caspase-12 was highly expressed from 8 h, with the highest expression found at 24 h in Western blotting results, which correlates to the initiation of apoptosis from ER stress response in the cell (Figure 5C). For Caspase proteins, post-translational cleavage is a dominant process to form active proteins, which happens on the membrane of different organelles. The overexpression of Caspase-12 at protein and mRNA level was observed at the same time (Figure S1A). Mitochondria may not be greatly involved in the cellular apoptosis which is induced by ZnO NPs treatment when comparing the quantity of cleaved Caspase-3 to -12, although its mRNA and prototype protein were all up-regulated

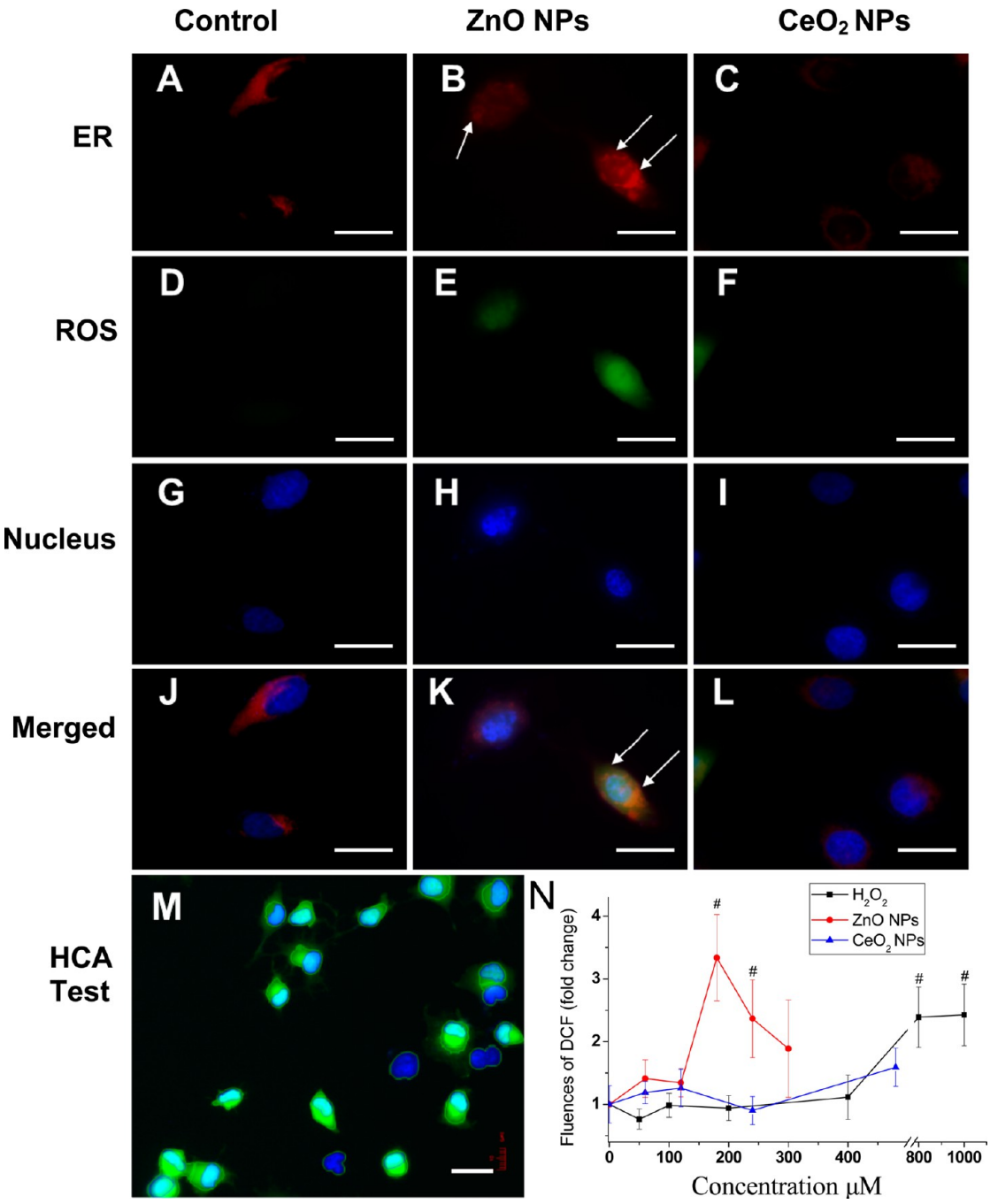

Figure 4. ROS levels in HUVECs after exposure to nanoparticles. (A−L) Fluorescence microscope observation of intracellular ROS induced by nanoparticles. HUVECs were treated with 240 μM ZnO NPs or CeO_2 NPs for 8 h, then, stained with ER Tracker Red dye and DCF-DA for simultaneously detection of ER and ROS by fluorescence microscope. (M) One image from ZnO NPs treatment group shows the segmentation process of high-content analysis (HCA) method. (N) Quantitative analysis of ROS level by HCA after HUVECs treated with nanoparticles for 8 h. Data expressed as mean ± SD, # $p < 0.01$ comparing to the in-plate control, $n = 6$. Bars = 10 μm. The white arrows show the bright and aggregated ER in ZnO NP treated cells.

at the same time by the stress response (Figure 5C and Figure S1A,B). Similarly, poly (ADP-ribose) polymerase 1 (PARP-1), one of the major nuclear targets for caspases that could be processed by activated caspase-3 to produce the 89 kDa fragment, did not show significant activation (Figure S1C).[41] Figure 3 shows that there is decreased amount of mitochondria observed by TEM, which means normal cellular functions may be impaired in order to counteract the stress from NPs. Further, the influences on the mitochondria are reported to be closely linked to the occurrence of ER stress.[42] Significant up-regulation of BiP protein gave the similar indication that ER stress response happens from 8 h after treatment as evidenced in the Western blotting results (Figure 5C). Further, the 70-kDa heat shock protein (HSP70) provided evidence of the increased stress condition in the cells after ZnO NPs treatment (Figure S1C). It is clearly shown that exposure to CeO_2 nanoparticles did not generate ER stress

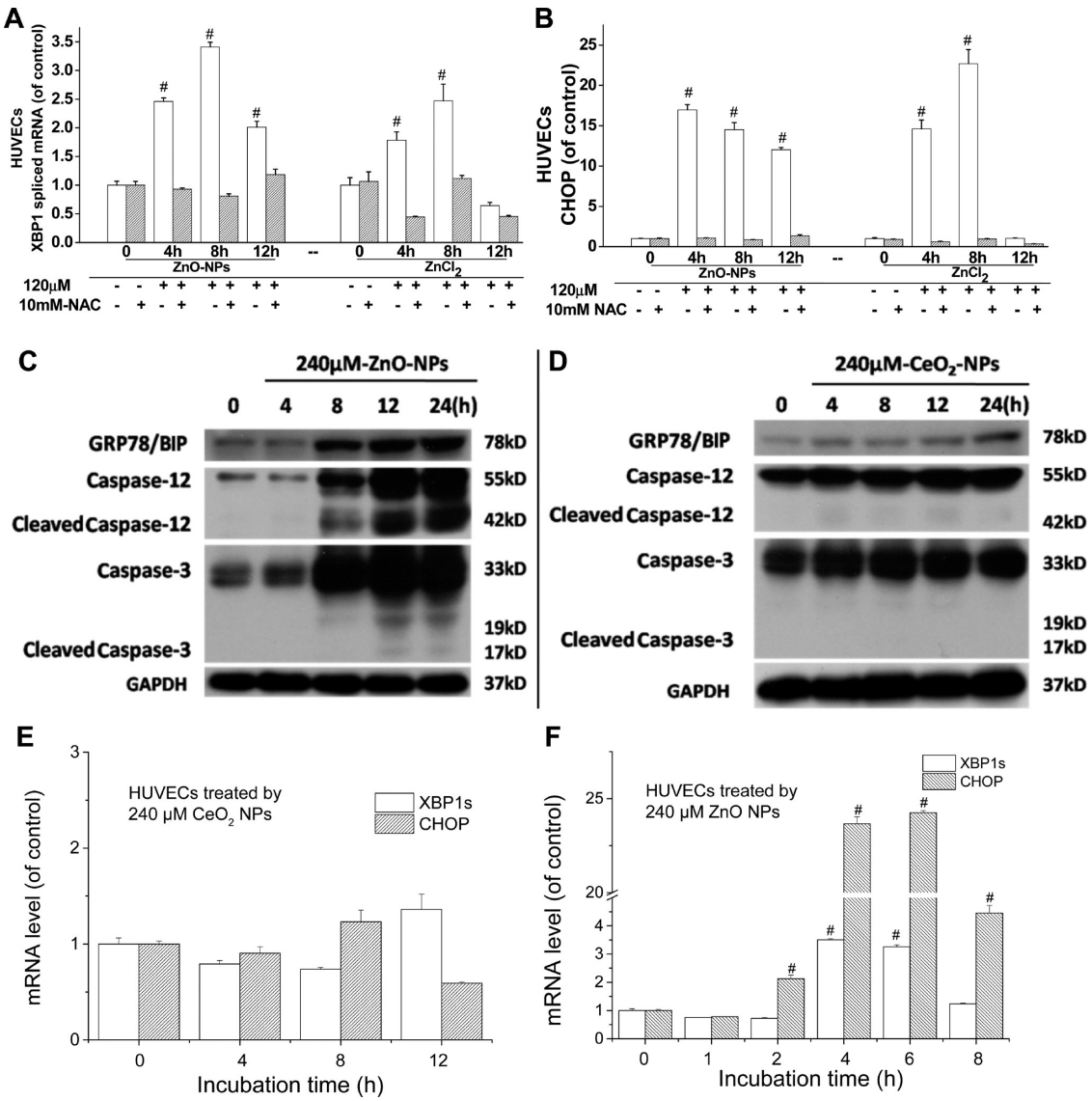

Figure 5. Induction of ER stress markers in HUVECs. (A and B) Time response of *xbp-1* splicing and *chop* mRNA level induced by ZnO NPs and $ZnCl_2$ at 120 μM concentration. A 10 mM NAC pretreatment was used as antioxidant to abolish the ROS accumulation. (C) Western blotting results of GRP78/BiP, Caspase-12 and Caspase-3 proteins when cells were treated with ZnO NPs, or (D) CeO_2 NPs at the dosage of 240 μM. (E) Time-dependent responses of *xbp-1s* and *chop* mRNA levels when incubating with 240 μM CeO_2 NPs, and (F) 240 μM ZnO NPs. The results are expressed as mean $\pm$ SD of at least 3 independent experiments. # $p < 0.01$ comparing to the control.

in HUVECs in the parallel test when treated at the dosage of 240 μM (Figure 5D,E). Moreover, CeO_2 NPs still have the possibility to influence the ER function by sustained incubation as illustrated by the slight up-regulation of BiP protein at 24 h in Western blotting results as shown in Figure 5D. Thus, we propose this slight activation of ER stress in CeO_2 NPs will have a beneficial effect of protecting the cell and counteracting the possible subsequent adverse effects and even apoptosis.

Dosage is a crucial factor when investigating the toxicity of materials. As ER stress is a sensitive marker for the interruption of cellular homeostasis, we suppose that the occurrence of toxicity outcomes could not bypass this cellular protecting response. From real-time PCR results of *xbp-1s* and *chop*, we found that the maximum peak of ER stress response had been shortened from 8 to 4 h by exposure to a dosage of 240 μM, unlike the profile at lower dosage of 120 μM which showed the response peak at 8 h with decreasing from 12 h (Figure 5A,B,F). At the meantime, we quantified the percentage of cells in early apoptotic or late apoptotic (necrotic) stages in HUVECs cells by flow cytometry (Table 2). High dosage of ZnO NPs (240 μM) induced significant apoptosis in 8 and 24 h time points, while 120 μM leaded negligible apoptosis. Sustained stress still takes more cells to apoptosis as illustrated in the comparison of 24 and 8 h earlier apoptosis and total death events. It means that the activation of ER stress is an earlier event and could be considered as a valuable predictive end point in the nanotoxicological study.

TABLE 2. Determination of Earlier Apoptotic and Total Cell Death Using Flow Cytometry after Incubating with ZnO and CeO_2 Nanoparticles[a]

particles	dose (μM)	exposure time (h)	early apoptosis (%)	death (%)
Control	0	24	1.20 ± 0.14	2.05 ± 0.30
ZnO	120	8	1.50 ± 0.17	3.29 ± 0.22
	120	24	2.14 ± 0.23	4.01 ± 0.29
	240	8	4.01 ± 0.52[#]	10.60 ± 0.80[#]
	240	24	8.16 ± 0.39[#]	25.63 ± 1.22[#]
CeO_2	240	8	1.24 ± 0.20	2.23 ± 0.37
	240	24	1.79 ± 0.18	3.36 ± 0.21

[a] Data expressed as mean ± SD, [#]$p < 0.01$, $n = 4$, One representative result from three independent experiments.

To understand the influences of NPs on the ER stress pathway, the gene expression profile was examined by PCR array. The threshold of differentially expressed with >2-fold change and values of $p < 0.05$ was used for the selection of genes for further analysis. It is shown that in total 84 genes were examined in the PCR array and most of genes were unchanged (Figure 6 and Table S2). However, several classical marker genes of the ER stress showed striking different gene profiles between ZnO and CeO_2 NPs treated HUVECs. Six genes were found significantly up-regulated by ZnO NP treatment (Figure 6A and Table S2). The *DDIT3/chop* gene gave the similar significant high expression level to the results of real-time PCR in this research, which means a good correlation of these mRNA quantitative methods (Figure 5B). The three up-regulated heat shock proteins (HSPs) genes were the following: Heat shock 70 kDa protein 1β (*HSPA1*β), Heat shock 70 kDa protein 4 (*HSPA4*), and Heat shock 105 kDa/110 kDa protein 1 (*HSPH1*). The up-regulation of HSP 70 protein was verified by the Western blotting analysis (Figure S1C) and cell-based immunofluorescent imaging (Figure 7). As the major components of molecular chaperones that facilitate protein folding, HSPs at a high expression level mean that cells were in the stage of ER stress response. At the meantime, another two important ER stress marker genes, DNA damage-inducible protein 34 (*GADD34/PPP1R15a*) and homocysteine-inducible, endoplasmic reticulum stress-inducible, ubiquitin-like domain member 1 (*HERPUD1*), were found significantly up-regulated. The associated Western blotting results were provided in Figure 6C. On the contrary, no ER stress related genes were overexpressed in the CeO_2 NPs treated HUVECs, which means that ER stress/UPR pathway was still inactivated (Figure 6B). Furthermore, synoviolin (*SYVN1*) attributed to E3 ubiquitin ligase and torsinA (*TOR1A*) attributed to AAA+ ATPase, usually playing active roles in ER-associated degradation when overloading misfolded proteins by UPR,[43] were found slightly decreased under CeO_2 NPs treatment. Another ER protein Mdg1/ERdj4 (DNAJB9), a mammalian chaperone that belongs to the HSP40 protein family,[44] was similarly down-regulated. Our data correlates with previous studies that CeO_2 NPs had antioxidant character, especially internalized nanoceria effectively attenuated the cellular ROS.[36,37,45]

For better understanding of the ZnO NPs induced ER stress, we looked into the dominant signaling pathways by testing on HUVECs and a commonly used Chinese Hamster Ovary (CHO) cell line. The concentration of the treatments were 240 μM for HUVECs and 120 μM for CHO cells based on the cell viability assay showing a lower LC50 in CHO cells (data not shown). Figure 6C indicates a clear activation of the PERK pathway including the phosphorylation of PERK and eIF2α, up-regulation of Chop, GADD34 of downstream effectors in these cell lines.

Addition of proteasome inhibitor MG132 during the last 2 h was used in an independent batch sample collection test to detect the short-lived GADD34 for preventing its degradation as previously reported.[46,47] ATF-6α only showed moderate activation of the cleaved 50 kDa fragment in HUVECs, which may come from the reason of weak signal of that antibody. It had been reported that HERP protein is strongly induced in response to ER stress, a condition where unfolded proteins accumulate in the ER.[48] In our test, HERP, similar to BiP protein, was significantly up-regulated upon ZnO NPs treatment for 8 h by Western blotting analysis (Figure 6C) and cell-based immunofluorescent images (Figure 7). Comparatively, HSP 70 was up-regulated and had obvious distribution in whole cytoplasm. The increase of HERP in the ER means the accumulation of the unfolded proteins after ZnO NPs treatment. In a protein translational efficacy interruption test, pretreatment cycloheximide for 30 min blocked the *xbp-1s* mRNA and the transcription of full length *xbp-1* counterpart at the same time, although it is usually thought as the specific protein translation inhibitor (Figure S2). Low serum culture condition usually was used to decrease the cellular proliferation progress and lower the normal functions of transcription and translation as evidenced by the decrease of the response from full length *xbp-1* mRNA transcription level under ZnO NPs treatment. However, the splicing did not show comparatively decrease of the *xbp-1s* mRNA even further considering the attenuation outcome of unfolded protein level caused from the overall reduction in protein synthesis from the starvation.[49] If the unfolded protein is the only/dominant part of the stimulation of ER stress, there should have been at least a similar decrease between the *xbp-1s* and *xbp-1* mRNA. Therefore, the different attenuation of the *xbp-1s* and *xbp-1* mRNA response to cotreatment of ZnO NPs and low serum culture condition suggested that the ER stress induced by ROS is partially involved with the unfolded proteins within the ER as well as other contributing factors participating in this signaling progress.

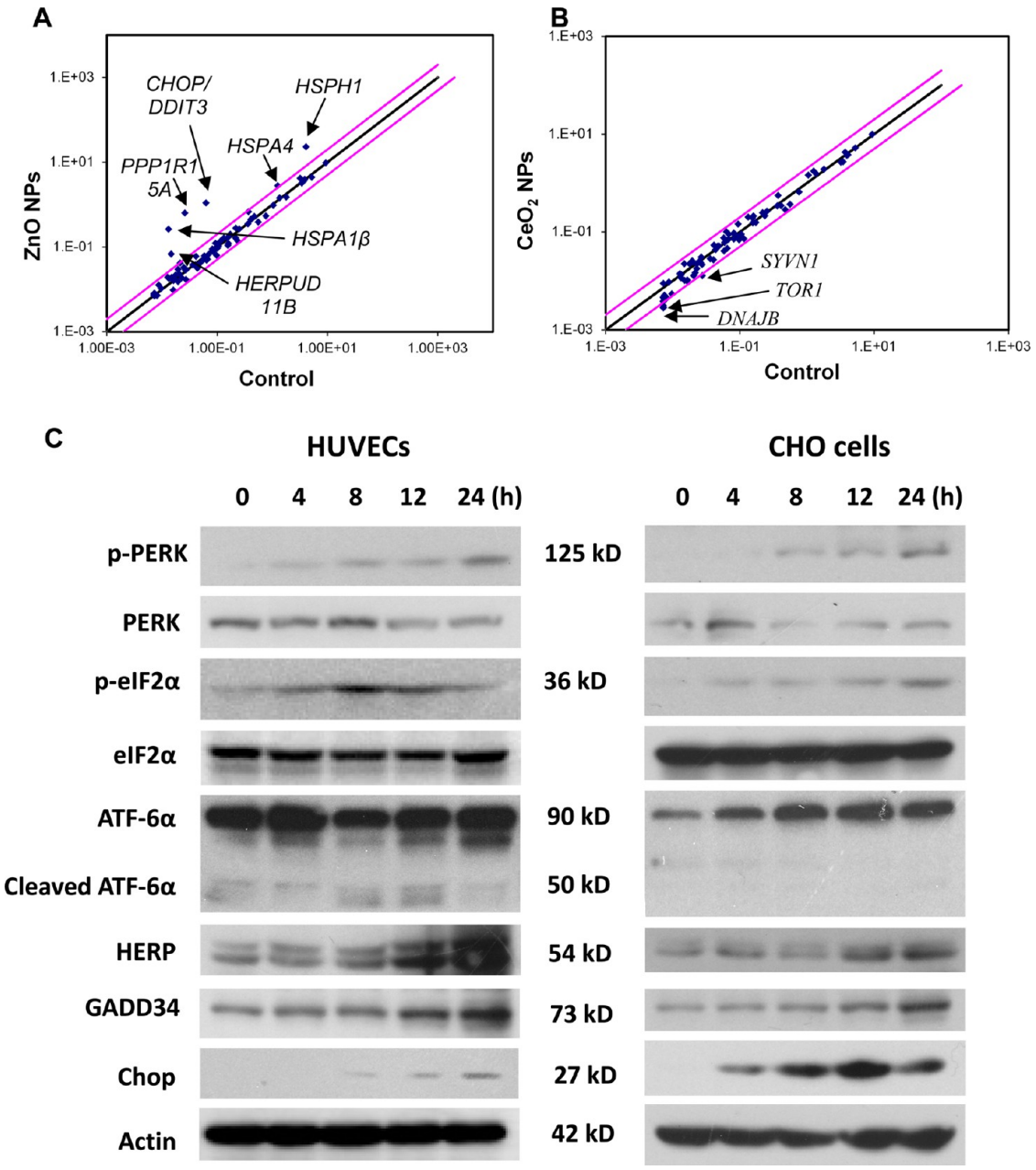

Figure 6. Scatterplots of PCR array and associated Western blotting analysis focusing on the ER stress signaling pathway. Scatterplots of expression levels of each gene in 240 μM (A) ZnO and (B) CeO_2 NPs incubated with HUVECs for 8 h *versus* blank control. The measurement was implemented on quantitative PCR machine using the PCR array kit (SABioscience company). The black line represents fold change of 1 and the pink lines indicate 2-fold change of gene expression threshold. (C) Western blotting analysis of HUVECs (240 μM) and CHO cells (120 μM) treated by ZnO NPs at indicated times.

ZnO NPs are fantastic for many applications of consumer products, and it is therefore necessary to assess the potential risks. In aqueous conditions, ZnO NPs have a high solubility and the maximum dissolved zinc concentration could be attained in complete DMEM is about 225 μM.[33] Further, higher than 80% of the maximum dissolved zinc could be reached within 3 h in normal culture conditions.[33,35] It is believed that Zn^{2+} solubilized from the NPs plays the major role of producing ROS and activating the ER stress under our adopted conditions in this research, of which ZnO NPs and $ZnCl_2$ have a very similar ER stress pathway outcome. Some reports show that ROS could lead to apoptosis and necrosis-like cell death mediated by early signals like ER stress, as well as activation of caspases and c-Jun N-terminal kinase (JNK), followed by mitochondrial dysfunction.[42,50] It is known that ER stress response is initiated to ameliorate the proper ER homeostasis. However, if these measures fail to reestablish the homeostasis, prolonged ER stress triggers the suicide machinery (Figure 8). The ER luminal chaperone BiP is one of the most general markers for a general induction of ER stress. We found significant up-regulation of BiP protein after exposure to ZnO

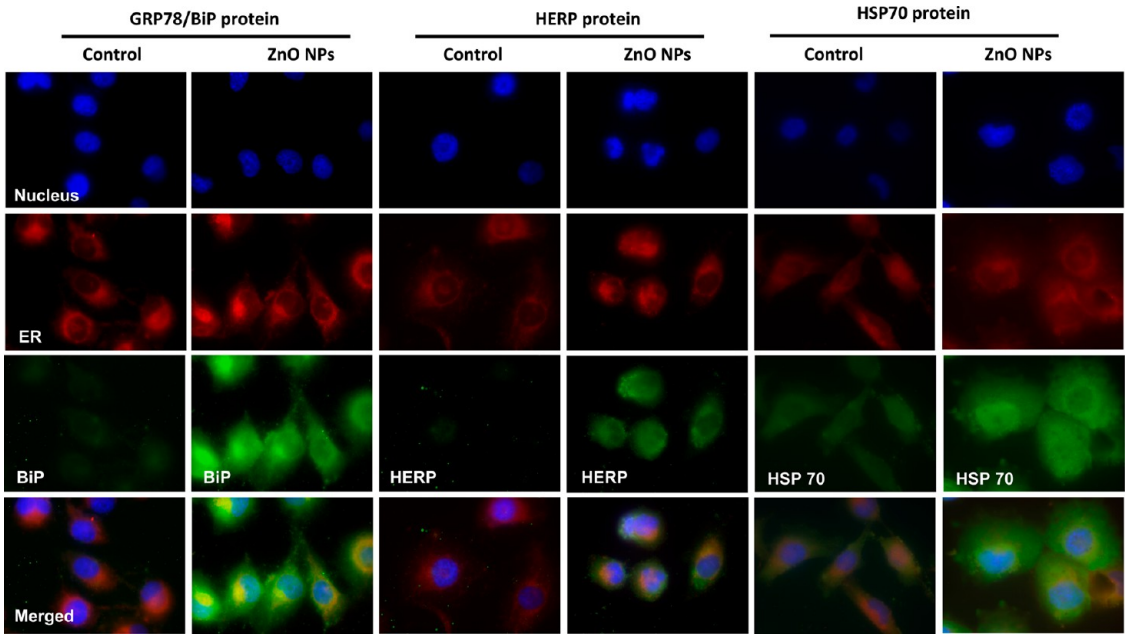

Figure 7. Immunofluorescent images of ER luminal chaperone BiP, HERP and HSP 70 proteins in HUVECs after incubating with 240 μM ZnO nanoparticles for 8 h. Hoechst and ER tracker were used to show the nucleus and ER, respectively.

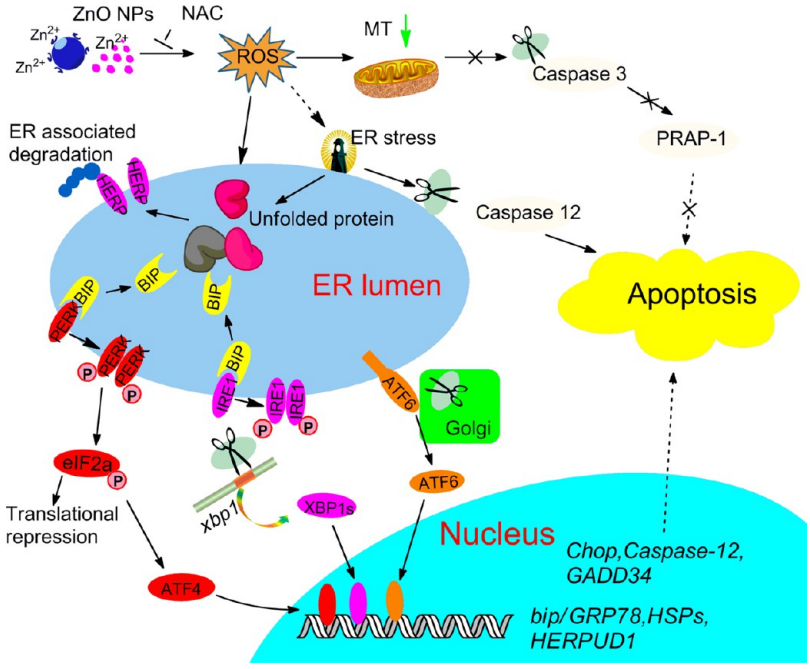

Figure 8. Schematic representation of the proposed mechanism for how ZnO NPs treatment influences the cellular homeostasis and activates the ER stress pathway.

nanoparticles, which leads stress-sensing proteins to an activated state, such as the activation and phosphorylation of PERK, and, in turn, the phosphorylation of eIF2α. The high activation of *xbp-1* regulates signal transduction and transcription factors. Thus, the present results indicate that PERK-eIF2α-ATF4-CHOP/GADD34 and IRE/XBP-1 pathways were fully activated in HUVECs by ZnO NPs treatment. Our experiments also show that ZnO NPs at higher concentration do not obviously activate Caspase 3 or PARP-1 and, accordingly, do not induce the mitochondrial-dependent apoptosis. In consequence, ZnO NPs at higher concentration activate Caspase-12-dependent ER stress pathways that eventually lead to cell apoptosis. Consistent with the findings in this research, the activation of ER stress response induced by ZnO NPs, at which the lower or nontoxic dosage is usually considered, could be thought as a warning or prelude to the following realistic damage outcomes.

Inhalation exposure of ZnO fumes can affect normal body functions. It had been reported that human

exposure to ZnO fumes with a mass median diameter (MMD) of 300 nm at 2.5 mg/m^3 for 2 h produced symptoms of metal fume fever, and the levels of the cytokine interleukin (IL)-6 in peripheral blood significantly increased.[51] A human clinical experiment study showed that inhalation exposure of ZnO fumes for only 10−30 min at a high concentration of 20−42 mg/m^3 increased the number of pro-inflammatory cytokines and neutrophils in bronchoalveolar lavage fluid (BALF).[52] In a rat exposure experiment, lower concentrations of ZnO NPs at occupationally relevant levels of 1.1−4.9 mg/m^3 and with longer inhalation time of 2 weeks can also generate the similar inflammation findings in the BALF.[53] NIOSH has recommended the permissible exposure limit of 5 mg/m^3 averaged over a work shift of up to 10 h per day, 40 h per week for the zinc oxide fume (NIOSH, Publication Number 0675). We estimated the lung deposition of ZnO NPs with MMD 150 nm of the particles used in this study. We found that even 64 min inhalation exposure at 1 mg/m^3 would lead to about 120 μM deposition concentration in the human lung lining fluid. This dosage was therefore used to detect the *in vitro* ER stress in present study. It means that ER stress effects could be used as a sensitive and earlier biomarker in the human occupational survey or *in vivo* inhalation test, *i.e.*, by testing on the cells collected from BALF or even mouth cavity. On the basis of its features of more definite, sensitive and earlier occurrence than other toxicological markers, we propose that ER stress would be considered as a valuable candidate of routine end point for future nanotoxicological study.

CONCLUSIONS

In this study, we investigated the toxicity and ER stress inducing ability of ZnO NPs in HUVECs compared to the Zn ions and CeO_2 NPs. Our results show that zinc ion solubilized from the surface of ZnO NP is important for its cytotoxicity in agreement with previous report.[35] ZnO NPs and the solubilized ions, but not CeO_2 NP, induce significant cellular ER stress or can be called UPR effects. ROS had been found to be involved in the induction of ER stress, for the reason that NAC pretreatment could thoroughly abolish this effect. Further, ER stress response usually happens at the noncytotoxic concentrations of ZnO NP before forming obvious adverse effects, which suggests that there is a possibility that cellular ER-stress could to be used as a sensitive and earlier marker for future nanotoxicological study. On the contrary, CeO_2 NPs did not show much stress on the cellular homeostasis, although a large number of NPs usually were accumulated in the cytoplasm after exposure. It had been shown in another *in vitro* study that CeO_2 NPs may enter into cells *via* a caveolin-1 and LAMP-1 endosomal compartment without invoking cytotoxic effects.[33] PCR array test shows ER stress pathway was widely activated by ZnO NPs treatment, with six of 84 tested marker genes significantly increased compared to CeO_2 NPs treatment. Further, the present results indicate that PERK-eIF2α-ATF4-CHOP/GADD34 pathway was fully activated in either HUVECs or commonly used CHO cells by ZnO NPs treatment.

Our research highlights the understanding of the toxic effects from NPs, especially that is meaningful to realize the stress of NPs hidden under the phenotype. Therefore, we propose that ER stress is a switch event for cellular destiny when studying the nanomaterial's exposure. However, the detailed mechanism of how ZnO NPs interrupt the cellular homeostasis and activate ER stress pathway is still required to be clarified in the future.

MATERIALS AND METHODS

Nanoparticles and Characterization. Two representative nanomaterials, ZnO (NM-110) and CeO_2 (NM-211), were supplied from Institute for Health and Consumer Protection (IHCP, one Joint Research Centre of European Commission located in Italy) for the project of European Commission seventh framework program. The NPs were provided under Good Laboratory Practice (GLP) conditions and preserved under argon in the dark until use.

Cell Culture and Cell Viability Assay. HUVECs and CHO cells were cultured at 37 °C in a 5% CO_2 atmosphere in Dulbecco's modified Eagle's medium (DMEM, Gibco) supplemented with 10% fetal bovine serum (FBS, Gibco). HUVECs were seeded at a density of 6×10^3 cells per well in 96-well plates in medium and incubated for 24 h. The medium was then replaced with 100 μL of medium containing various equivalent concentrations of $ZnCl_2$ (Sigma-Aldrich) chemical, ZnO or CeO_2 NPs. The cells were incubated for 24 h and cytotoxicity was measured using CCK-8 Kits (Dojindo Molecular Technologies, Tokyo, Japan) according to the manufacturer's protocol. The absorbance was measured at 450 nm with a reference at 600 nm using Infinite M200 microplate reader (Tecan, Durham).

Measurement of Apoptosis and Necrosis. HUVECs were preincubated for 24 h in 6-well plates in a humidified incubator (37 °C, 5% CO_2). Then the medium was replaced with 2 mL of medium containing various equivalent concentrations of ZnO and CeO_2 NPs for 8 and 24 h. Cells were washed three times with PBS and harvested. Then the double-stained annexin V-FITC Kit, which contained annexin V-FITC and propidium iodide solution (BD Biosciences), was used to incubate the cells, which were then analyzed using a Cell Lab Quanta SC flow cytometry (Beckman Coulter, 488 nm, FL1).

Detection of ROS Levels by Fluorescence Microscope. Cells were cultured on 35 mm Petri dishes for 24 h and treated with 240 μM ZnO and CeO_2 for the following 8 h. Cells in dishes were then washed with PBS and incubated separately for 30 min in complete medium with 1 μM ER Tracker Red dye probe, 5 μM ROS probe DCFH-DA and 1 μM nuclear probe Hoechst. These probes were purchased from Molecular Probes, Inc. After the medium was removed, cells were washed with PBS and fresh complete medium was added. The stained cells were observed and analyzed by fluorescence microscope (Olympus BX61W1 with Fluoview FV1000 software, Japan).

High Content Analysis on Cellular ROS Level. HUVECs were cultured at a density of 8×10^3 cells per well in 96-well plates in medium and maintained for 24 h. Adhered cells were incubated in complete medium with different concentrations of ZnO NPs for 8 h. Then, different groups of cells were costained with Hoechst 33342 and 10 μM ROS probe DCFH-DA in PBS solution

with 0.4% glucose for 30 min. H_2O_2 treated cells were used as a positive control. Cells were washed three times with PBS and IN cell analyzer 2000 (GE Health) was used to capture images. In each well, 9 image fields were captured at the same exposure time and at least 200 cells per image field were measured for effective data output. For each measured cells, the following calculations were performed automatically by the software IN cell analyzer 3.7.1 (GE Health). Target cells were assigned with marking on the Hoechst stained nuclear space at the DAPI channel; average florescence intensity was calculated by dividing the brightness of the entire field of target cells to the according area (Figure 4M). The cellular florescence intensity is used to reflect the accumulated ROS amount within the cell. More information can be found in our recent paper on the application of this technique.[54]

RNA Isolation, Reverse-Transcription PCR, and Quantitative Real-Time PCR. HUVECs cultured with medium for 24 h in 6-well plates. Then the medium was replaced with 2 mL of medium containing various equivalent concentrations of $ZnCl_2$, ZnO and CeO_2 NPs for 0, 4, 8, 12, and 24 h with or without 10 mM, 30 min sulfhydryl antioxidant NAC pretreatment; cells were washed 3 times with PBS and 1 mL of Trizol Reagent was added to each well to extract RNA according the Trizol protocol. After quantification of the extracted RNA pellets, aliquot samples were then reverse-transcribed to cDNA using Oligo dT (Promega). The resulting cDNA samples were analyzed by regular reverse-transcription PCR or quantitative real-time PCR (Eppendorf, Germany) using SYBR green as fluorescence dye, as described previously.[6] The DNA product amplified by *xbp-1* (Gel PCR) primer was analyzed by 3% agarose gel. The following genes were measured by real-time PCR: *xbp-1s*, *xbp-1*, *chop*, *caspase-3*, *caspase-12*, *gapdh*. All primer sequences were listed in Supporting Information Table S1.

Western Blotting. HUVECs cultured with medium for 24 h in 6-well plates. Then the medium was replaced with 2 mL of medium containing 240 μM ZnO and CeO_2 NPs for 0, 4, 8, 12, and 24 h; cells were washed 3 times with PBS, harvested with a scraper, and centrifuged at 2000*g* for 10 min at 4 °C. After discarding the supernatant, cells were lysed to collect the cellular proteins. Equal amounts (50 μg) of proteins were separated on 10% SDS-PAGE gels and transferred to nitrocellulose membranes. The membranes were blocked with 5% nonfat milk in TBST at room temperature. The primary antibody was used at 1:1000 dilution and the secondary antibody was used at 1:5000 dilution. Blots were developed using ECL (enhanced chemiluminescence) solution. The primary antibody of anti-CHOP is from Cell Signaling Technology, Inc. and all other antibodies (HSP 70, HERP, BiP, chop, caspase-3, caspase-12, PERK, eIF2α, ATF-6α and so on) in this research are purchased from Santa Cruz, Inc.

Quantitative Measurement of Cellular Uptake of Nanoparticles by ICP-MS. The inductively coupled plasma mass spectrometry (ICP-MS) was used to measure the cellular elemental contents after treatment with NPs or associated ions. HUVECs were seeded at a density of 1×10^5 cells per well in 6-well plates in medium and incubated for 24 h in an incubator at 37 °C, 5% CO_2 and 10% humidity, then the medium was removed and fresh complete medium containing different concentrations NPs were added to plates for the nanoparticles internalization experiment. Cells were incubated for different durations (6, 12, 24 h), four dishes of cells being used at each time point. Cells in each dish were washed gently with PBS three times, digested with 0.25% trypsin containing 0.02% EDTA, centrifuged for 5 min at 1500 rpm, then collected and counted. After cell sample collection, 3 mL of HNO_3 was added to each centrifuge tube for predigestion overnight. The next day, the solution was transferred into a conical flask and 2 mL 30% H_2O_2 was added. The flasks were placed onto a hot plate and maintained at 150 °C for 3 h until digestion was complete. Then samples were taken out and cooled to room temperature. The solution volume was diluted to 3 mL with a solution containing 2% HNO_3 and 1% HCL. A total of 10 ng/mL (ppb) bismuth (Bi) was used as an internal standard. Both standard and test solutions were measured for three times by ICP-MS.

Subcellular Ultrastructure and Localization of Nanoparticles by TEM. HUVECs were preincubated for 24 h in 60 mm Petri dishes at 37 °C in a 5% CO_2 atmosphere. After incubation with medium containing different concentrations of ZnO and CeO_2 NPs for 8 h, cells were harvested and washed with PBS three times. Cell pellets were fixed overnight in a fixation solution containing 2.5% glutaraldehyde in 0.1 M PBS. Pellets were then postfixed with 1% OsO_4 in PBS for 1 h, dehydrated in a graded series of ethanol, treated with propylene oxide, and embedded in Epon. Approximately 80 nm thick sections were cut, placed on carbon film supported by copper grids, stained with uranyl acetate and lead citrate, and observed with a transmission electron microscope (H-600, Hitachi, Japan) at 80 kV.

Transcriptional Profiling. The relative expression of 84 genes represented in the human Unfolded Protein Response Plus PCR Array (SABioscience) was determined using RNA isolated from NPs treated and nontreated HUVECs. Total RNA was isolated using the TRIzol reagent (Invitrogen, Carlsbad CA). The cDNA was prepared using SABioscience RT^2 First Strand Kit and RT^2 Sybr qPCR Master Mix according to manufacturer's instructions (Qiagen, Germany). Three PCR array repeats were done using quantitative real-time PCR (Mastercycler ep realplex^4, Eppendorf). Data was analyzed using SABioscience RT^2 Profiler analysis software, with nontreated HUVECs samples serving as control. The threshold of differential expression with >2-fold change and values of $p < 0.05$ was used as the statistical significance.

Cell-Based Immunofluorescence Assay. Cells were rinsed twice in PBS, fixed with 4% paraformaldehyde for 1 h, permeabilized with 0.1% Triton in PBS for 20 min, blocked with 10% goat serum in PBS for 1 h followed by incubation with primary antibody for at least 2 h, washed three times with PBS, and incubated with fluorescently labeled secondary antibody (1:500 dilution for 1 h) followed by Hoechst and ER tracker, as above-described. Coverslips were mounted after three times washing with PBS. Images for morphological analysis were acquired under an Olympus inverted microscope (BX61W1) with a 100× oil immersion objective.

Estimation on the Lung Deposition of ZnO NPs of Inhalation Exposure. The basic procedure was adopted according to a recently published paper on dosimetry calculation.[55] Briefly, alveolar deposition efficiency of ZnO NPs used in this paper is 14% that was determined with the following parameters by Multiple-Path Particle Dosimetry Model (MPPD, Applied Research Associates, Inc., Albuquerque, NM) 2.11 software. MMD (equal to Count Median Diameter, CMD when using monodispersed aerosol), 150 nm; geometric standard diameter (GSD), 1.0 and assuming a monodispersed aerosol and a single mode distribution. Human alveolar deposition could be calculated by the equation: human alveolar deposition = Airborne Concentration × V_E × exposure duration × alveolar deposition efficiency. For example, if inhalation exposure at 1 mg/m^3 for 64 min, human alveolar deposition will be 0.177 mg, *i.e.*, 1 mg/m^3 × 20 L/min × 10^{-3} m^3/L × 64 min ×14% = 0.177 mg. An average volume of 18.2 mL for lung lining fluid of a person weighting 70 kg was assumed in the calculation, although the lung lining fluid had been given a SD, 0.26 (±0.1) mL/kg.[56] The quantity of 0.177 mg from exposure for 64 min in 1 mg/m^3 environment gives a lung deposition of 120 μM which used in the *in vitro* detection of ER stress in this research. It should be noted here the use of the MMD/CMD but not the mass median aerodynamic diameter (MMAD) in the calculation. The alveolar deposition efficiency will increase from 14% to about 25% if directly using 150 nm as the MMAD in the calculation, which means only 35 min required by exposure to 1 mg/m^3 concentration for the lung to obtaining equal deposition of 120 μM.

Conflict of Interest: The authors declare no competing financial interest.

Acknowledgment. We thank the financial support from the Ministry of Science and Technology of China (2011CB933401 and 2012CB934003), National Natural Science Foundation of China (21277080 and 21320102003), National Major Scientific Instruments Development Project (2011YQ03013406), International Science & Technology Cooperation Program of China, Ministry of Science and Technology of China (2013DFG32340 and 2014DFG52500), and the European Commission through the Seventh Framework Programme for Research and Technological Development (MARINA 263215).

Supporting Information Available: Additional three figures and two tables, as referenced in the main text including figures of mRNA levels of *caspase-3* and *-12* after ZnO NPs treatment, Western results of PARP-1 and HSP 70, ER stress interruption test, tables of PCR primer information and 84 gene expression results of PCR array. This material is available free of charge *via* the Internet at http://pubs.acs.org.

REFERENCES AND NOTES

1. Nalwa, H.; Zhao, Y. *Nanotoxicology*; American Scientific Publishers: Valencia, CA, 2007.
2. Chen, R.; Chen, C. Nanotoxicity. In *The Nanobiotechnology Handbook*; Xie, Y., Ed.; Taylor & Francis: New York. 2012; pp 599−620.
3. Oberdorster, G.; Oberdorster, E.; Oberdorster, J. Nanotoxicology: An Emerging Discipline Evolving from Studies of Ultrafine Particles. *Environ. Health. Perspect.* **2005**, *113*, 823–839.
4. Ge, C.; Du, J.; Zhao, L.; Wang, L.; Liu, Y.; Li, D.; Yang, Y.; Zhou, R.; Zhao, Y.; Chai, Z.; *et al.* Binding of Blood Proteins to Carbon Nanotubes Reduces Cytotoxicity. *Proc. Natl. Acad. Sci. U.S.A.* **2011**, *108*, 16968–16973.
5. Ge, C.; Meng, L.; Xu, L.; Bai, R.; Du, J.; Zhang, L.; Li, Y.; Chang, Y.; Zhao, Y.; Chen, C. Acute Pulmonary and Moderate Cardiovascular Responses of Spontaneously Hypertensive Rats after Exposure to Single-Wall Carbon Nanotubes. *Nanotoxicology* **2012**, *6*, 526–542.
6. Meng, L.; Chen, R.; Jiang, A.; Wang, L.; Wang, P.; Li, C. Z.; Bai, R.; Zhao, Y.; Autrup, H.; Chen, C. Short Multiwall Carbon Nanotubes Promote Neuronal Differentiation of PC12 Cells *via* Up-Regulation of the Neurotrophin Signaling Pathway. *Small* **2013**, *9*, 1786–1798.
7. Meng, L.; Jiang, A.; Chen, R.; Li, C. Z.; Wang, L.; Qu, Y.; Wang, P.; Zhao, Y.; Chen, C. Inhibitory Effects of Multiwall Carbon Nanotubes with High Iron Impurity on Viability and Neuronal Differentiation in Cultured PC12 Cells. *Toxicology* **2013**, *313*, 49–58.
8. Qu, Y.; Li, W.; Zhou, Y.; Liu, X.; Zhang, L.; Wang, L.; Li, Y. F.; Iida, A.; Tang, Z.; Zhao, Y.; *et al.* Full Assessment of Fate and Physiological Behavior of Quantum Dots Utilizing Caenorhabditis Elegans as a Model Organism. *Nano Lett.* **2011**, *11*, 3174–3183.
9. Boyes, W. K.; Chen, R.; Chen, C.; Yokel, R. A. The Neurotoxic Potential of Engineered Nanomaterials. *Neurotoxicology* **2012**, *33*, 902–910.
10. Maurer-Jones, M. A.; Gunsolus, I. L.; Murphy, C. J.; Haynes, C. L. Toxicity of Engineered Nanoparticles in the Environment. *Anal. Chem.* **2013**, *85*, 3036–3049.
11. Chen, Z.; Meng, H.; Xing, G.; Chen, C.; Zhao, Y.; Jia, G.; Wang, T.; Yuan, H.; Ye, C.; Zhao, F.; *et al.* Acute Toxicological Effects of Copper Nanoparticles *in Vivo*. *Toxicol. Lett.* **2006**, *163*, 109–120.
12. Wang, J.; Zhou, G.; Chen, C.; Yu, H.; Wang, T.; Ma, Y.; Jia, G.; Gao, Y.; Li, B.; Sun, J.; *et al.* Acute Toxicity and Biodistribution of Different Sized Titanium Dioxide Particles in Mice after Oral Administration. *Toxicol. Lett.* **2007**, *168*, 176–185.
13. Zhang, L.; Bai, R.; Liu, Y.; Meng, L.; Li, B.; Wang, L.; Xu, L.; Le Guyader, L.; Chen, C. The Dose-Dependent Toxicological Effects and Potential Perturbation on the Neurotransmitter Secretion in Brain Following Intranasal Instillation of Copper Nanoparticles. *Nanotoxicology* **2011**, *6*, 562–575.
14. Bai, R.; Zhang, L.; Liu, Y.; Meng, L.; Wang, L.; Wu, Y.; Li, W.; Ge, C.; Le Guyader, L.; Chen, C. Pulmonary Responses to Printer Toner Particles in Mice after Intratracheal Instillation. *Toxicol. Lett.* **2010**, *199*, 288–300.
15. Wang, P.; Nie, X.; Wang, Y.; Li, Y.; Ge, C.; Zhang, L.; Wang, L.; Bai, R.; Chen, Z.; Zhao, Y.; *et al.* Multiwall Carbon Nanotubes Mediate Macrophage Activation and Promote Pulmonary Fibrosis through TGF-Beta/Smad Signaling Pathway. *Small* **2013**, *9* (22), 3799–3811.
16. Roussel, B. D.; Kruppa, A. J.; Miranda, E.; Crowther, D. C.; Lomas, D. A.; Marciniak, S. J. Endoplasmic Reticulum Dysfunction in Neurological Disease. *Lancet. Neurol.* **2013**, *12*, 105–118.
17. Garg, A. D.; Kaczmarek, A.; Krysko, O.; Vandenabeele, P.; Krysko, D. V.; Agostinis, P. ER Stress-Induced Inflammation: Does It Aid or Impede Disease Progression? *Trends Mol Med.* **2012**, *18*, 589–598.
18. Lin, J. H.; Walter, P.; Yen, T. S. Endoplasmic Reticulum Stress in Disease Pathogenesis. *Annu. Rev. Pathol.* **2008**, *3*, 399–425.
19. Yoshida, H.; Matsui, T.; Yamamoto, A.; Okada, T.; Mori, K. XBP1 mRNA Is Induced by ATF6 and Spliced by IRE1 in Response to ER Stress To Produce a Highly Active Transcription Factor. *Cell* **2001**, *107*, 881–891.
20. Lin, J. H.; Li, H.; Yasumura, D.; Cohen, H. R.; Zhang, C.; Panning, B.; Shokat, K. M.; Lavail, M. M.; Walter, P. IRE1 Signaling Affects Cell Fate during the Unfolded Protein Response. *Science* **2007**, *318*, 944–949.
21. Nakagawa, T.; Zhu, H.; Morishima, N.; Li, E.; Xu, J.; Yankner, B. A.; Yuan, J. Caspase-12 Mediates Endoplasmic-Reticulum-Specific Apoptosis and Cytotoxicity by Amyloid-Beta. *Nature* **2000**, *403*, 98–103.
22. Van Schadewijk, A.; van't Wout, E. F.; Stolk, J.; Hiemstra, P. S. A Quantitative Method for Detection of Spliced X-Box Binding Protein-1 (XBP1) mRNA as a Measure of Endoplasmic Reticulum (ER) Stress. *Cell Stress Chaperones* **2012**, *17*, 275–279.
23. Budihardjo, I.; Oliver, H.; Lutter, M.; Luo, X.; Wang, X. Biochemical Pathways of Caspase Activation during Apoptosis. *Annu. Rev. Cell Dev. Biol.* **1999**, *15*, 269–290.
24. Sarkar, A.; Das, J.; Manna, P.; Sil, P. C. Nano-Copper Induces Oxidative Stress and Apoptosis in Kidney *via* Both Extrinsic and Intrinsic Pathways. *Toxicology* **2011**, *290*, 208–217.
25. Siddiqui, M. A.; Alhadlaq, H. A.; Ahmad, J.; Al-Khedhairy, A. A.; Musarrat, J.; Ahamed, M. Copper Oxide Nanoparticles Induced Mitochondria Mediated Apoptosis in Human Hepatocarcinoma Cells. *PLoS One* **2013**, *8*, e69534.
26. Christen, V.; Capelle, M.; Fent, K. Silver Nanoparticles Induce Endoplasmatic Reticulum Stress Response in Zebrafish. *Toxicol. Appl. Pharmacol.* **2013**, *272*, 519–528.
27. Zhang, R.; Piao, M. J.; Kim, K. C.; Kim, A. D.; Choi, J. Y.; Choi, J.; Hyun, J. W. Endoplasmic Reticulum Stress Signaling Is Involved in Silver Nanoparticles-Induced Apoptosis. *Int. J. Biochem. Cell Biol.* **2012**, *44*, 224–232.
28. Christen, V.; Capelle, M.; Fent, K. Silver Nanoparticles Induce Endoplasmatic Reticulum Stress Response in Zebrafish. *Toxicol. Appl. Pharmacol.* **2013**, *272*, 519–528.
29. Nel, A.; Xia, T.; Madler, L.; Li, N. Toxic Potential of Materials at the Nanolevel. *Science* **2006**, *311*, 622–627.
30. Tsai, Y. Y.; Huang, Y. H.; Chao, Y. L.; Hu, K. Y.; Chin, L. T.; Chou, S. H.; Hour, A. L.; Yao, Y. D.; Tu, C. S.; Liang, Y. J.; *et al.* Identification of the Nanogold Particle-Induced Endoplasmic Reticulum Stress by Omic Techniques and Systems Biology Analysis. *ACS Nano* **2011**, *5*, 9354–9369.
31. Christen, V.; Fent, K. Silica Nanoparticles and Silver-Doped Silica Nanoparticles Induce Endoplasmatic Reticulum Stress Response and Alter Cytochrome P4501A Activity. *Chemosphere* **2012**, *87*, 423–434.
32. Piccinno, F.; Gottschalk, F.; Seeger, S.; Nowack, B. Industrial Production Quantities and Uses of Ten Engineered Nanomaterials in Europe and the World. *J. Nanopart. Res.* **2012**, *14*, 1109–1119.
33. Xia, T.; Kovochich, M.; Liong, M.; Madler, L.; Gilbert, B.; Shi, H.; Yeh, J. I.; Zink, J. I.; Nel, A. E. Comparison of the Mechanism of Toxicity of Zinc Oxide and Cerium Oxide Nanoparticles Based on Dissolution and Oxidative Stress Properties. *ACS Nano* **2008**, *2*, 2121–2134.
34. Xia, T.; Zhao, Y.; Sager, T.; George, S.; Pokhrel, S.; Li, N.; Schoenfeld, D.; Meng, H.; Lin, S.; Wang, X.; *et al.* Decreased Dissolution of Zno by Iron Doping Yields Nanoparticles with Reduced Toxicity in the Rodent Lung and Zebrafish Embryos. *ACS Nano* **2011**, *5*, 1223–1235.
35. Yang, S. T.; Liu, J. H.; Wang, J.; Yuan, Y.; Cao, A.; Wang, H.; Liu, Y.; Zhao, Y. Cytotoxicity of Zinc Oxide Nanoparticles: Importance of Microenvironment. *J. Nanosci. Nanotechnol.* **2010**, *10*, 8638–8645.
36. Celardo, I.; Pedersen, J. Z.; Traversa, E.; Ghibelli, L. Pharmacological Potential of Cerium Oxide Nanoparticles. *Nanoscale* **2011**, *3*, 1411–1420.

37. Kim, C. K.; Kim, T.; Choi, I. Y.; Soh, M.; Kim, D.; Kim, Y. J.; Jang, H.; Yang, H. S.; Kim, J. Y.; Park, H. K.; *et al.* Ceria Nanoparticles That Can Protect against Ischemic Stroke. *Angew. Chem., Int. Ed.* **2012**, *51*, 11039–11043.
38. Moreau, J. W.; Weber, P. K.; Martin, M. C.; Gilbert, B.; Hutcheon, I. D.; Banfield, J. F. Extracellular Proteins Limit the Dispersal of Biogenic Nanoparticles. *Science* **2007**, *316*, 1600–1603.
39. D'Autreaux, B.; Toledano, M. B. ROS as Signalling Molecules: Mechanisms That Generate Specificity in ROS Homeostasis. *Nat. Rev. Mol. Cell Biol.* **2007**, *8*, 813–824.
40. Ray, P. D.; Huang, B. W.; Tsuji, Y. Reactive Oxygen Species (ROS) Homeostasis and Redox Regulation in Cellular Signaling. *Cell. Signalling* **2012**, *24*, 981–990.
41. D'Amours, D.; Sallmann, F. R.; Dixit, V. M.; Poirier, G. G. Gain-of-Function of Poly(ADP-ribose) Polymerase-1 upon Cleavage by Apoptotic Proteases: Implications for Apoptosis. *J. Cell Sci.* **2001**, *114*, 3771–3778.
42. Barateiro, A.; Vaz, A. R.; Silva, S. L.; Fernandes, A.; Brites, D. ER Stress, Mitochondrial Dysfunction and Calpain/JNK Activation Are Involved in Oligodendrocyte Precursor Cell Death by Unconjugated Bilirubin. *Neuromol. Med.* **2012**, *14*, 285–302.
43. Nery, F. C.; Armata, I. A.; Farley, J. E.; Cho, J. A.; Yaqub, U.; Chen, P.; da Hora, C. C.; Wang, Q.; Tagaya, M.; Klein, C.; *et al.* Torsina Participates in Endoplasmic Reticulum-Associated Degradation. *Nat. Commun.* **2011**, *2*, 393.
44. Berger, B. J.; Muller, T. S.; Buschmann, I. R.; Peters, K.; Kirsch, M.; Christ, B.; Prols, F. High Levels of the Molecular Chaperone Mdg1/Erdj4 Reflect the Activation State of Endothelial Cells. *Exp. Cell Res.* **2003**, *290*, 82–92.
45. Chen, S.; Hou, Y.; Cheng, G.; Zhang, C.; Wang, S.; Zhang, J. Cerium Oxide Nanoparticles Protect Endothelial Cells from Apoptosis Induced by Oxidative Stress. *Biol. Trace Elem. Res.* **2013**, *154*, 156–166.
46. Brush, M. H.; Shenolikar, S. Control of Cellular GADD34 Levels by the 26S Proteasome. *Mol. Cell. Biol.* **2008**, *28*, 6989–7000.
47. Clavarino, G.; Claudio, N.; Dalet, A.; Terawaki, S.; Couderc, T.; Chasson, L.; Ceppi, M.; Schmidt, E. K.; Wenger, T.; Lecuit, M.; Gatti, E.; Pierre, P. Protein Phosphatase 1 Subunit Ppp1r15a/GADD34 Regulates Cytokine Production In Polyinosinic:Polycytidylic Acid-Stimulated Dendritic Cells. *Proc. Natl. Acad. Sci. U.S.A.* **2012**, *109*, 3006–3011.
48. Schroder, M.; Kaufman, R. J. The Mammalian Unfolded Protein Response. *Annu. Rev. Biochem.* **2005**, *74*, 739–789.
49. Damiano, F.; Alemanno, S.; Gnoni, G. V.; Siculella, L. Translational Control of the Sterol-Regulatory Transcription Factor SREBP-1 mRNA in Response to Serum Starvation or ER Stress Is Mediated by an Internal Ribosome Entry Site. *Biochem. J.* **2010**, *429*, 603–612.
50. Jiang, C.; Zhang, S.; Liu, H.; Zeng, Q.; Xia, T.; Chen, Y.; Kuang, G.; Zhao, G.; Wu, X.; Zhang, X.; *et al.* The Role of the IRE1 Pathway in PBDE-47-Induced Toxicity in Human Neuroblastoma SH-SY5Y Cells *in Vitro*. *Toxicol. Lett.* **2012**, *211*, 325–333.
51. Fine, J. M.; Gordon, T.; Chen, L. C.; Kinney, P.; Falcone, G.; Beckett, W. S. Metal Fume Fever: Characterization of Clinical and Plasma IL-6 Responses in Controlled Human Exposures to Zinc Oxide Fume at and below the Threshold Limit Value. *J. Occup. Environ. Med.* **1997**, *39*, 722–726.
52. Kuschner, W. G.; D'Alessandro, A.; Wong, H.; Blanc, P. D. Early Pulmonary Cytokine Responses to Zinc Oxide Fume Inhalation. *Environ. Res.* **1997**, *75*, 7–11.
53. Chuang, H. C.; Juan, H. T.; Chang, C. N.; Yan, Y. H.; Yuan, T. H.; Wang, J. S.; Chen, H. C.; Hwang, Y. H.; Lee, C. H.; Cheng, T. J. Cardiopulmonary Toxicity of Pulmonary Exposure to Occupationally Relevant Zinc Oxide Nanoparticles. *Nanotoxicology* **2014**, *8*, 593–604.
54. Huo, L.; Chen, R.; Shi, X.; Bai, R.; Wang, P.; Chang, Y.; Chen, C. High-Content Screening for Assessing Nanomaterial Toxicity. *J. Nanosci. Nanotechnol.* **2013**, 10.1166/jnn.2014.9032.
55. Erdely, A.; Dahm, M.; Chen, B. T.; Zeidler-Erdely, P. C.; Fernback, J. E.; Birch, M. E.; Evans, D. E.; Kashon, M. L.; Deddens, J. A.; Hulderman, T.; Bilgesu, S. A.; Battelli, L.; Schwegler-Berry, D.; Leonard, H. D.; McKinney, W.; Frazer, D. G.; Antonini, J. M.; Porter, D. W.; Castranova, V.; Schubauer-Berigan, M. K. Carbon Nanotube Dosimetry: from Workplace Exposure Assessment to Inhalation Toxicology. *Part. Fibre Toxicol.* **2013**, *10*, 53.
56. Noppen, M.; De Waele, M.; Li, R.; Gucht, K. V.; D'Haese, J.; Gerlo, E.; Vincken, W. Volume and Cellular Content of Normal Pleural Fluid in Humans Examined by Pleural Lavage. *Am. J. Respir. Crit. Care Med.* **2000**, *162*, 1023–1026.